NANO LETTERS

Letter

pubs.acs.org/NanoLett

Electron Tomography Resolves a Novel Crystal Structure in a Binary Nanocrystal Superlattice

Mark P. Boneschanscher,[†,⊥] Wiel H. Evers,[†,⊥,∥] Weikai Qi,[‡] Johannes D. Meeldijk,[§] Marjolein Dijkstra,[‡] and Daniel Vanmaekelbergh*[,†]

[†]Condensed Matter and Interfaces and [‡]Soft Condensed Matter, Debye Institute for Nanomaterials Science, University Utrecht, Princetonplein 1, 3584 CC Utrecht, The Netherlands

[§]Electron Microscopy Group, Utrecht University, Padualaan 8, 3584 CH Utrecht, The Netherlands

Supporting Information

ABSTRACT: The self-assembly of different nanocrystals into a binary superlattice is of interest for both colloidal science and nanomaterials science. New properties may emerge from the interaction between the nanocrystal building blocks that are ordered in close contact in three dimensions. Identification of the superlattice structure including its defects is of key interest in understanding the electrical and optical properties of these systems. Transmission electron microscopy (TEM) has been very instrumental to reach this goal but fails for complex crystal structures and buried defects. Here, we use electron tomography to resolve the three-dimensional crystal structure of a binary superlattice that could not be resolved by TEM only. The structure with a $[PbSe]_6[CdSe]_{19}$ stoichiometry has no analogue in the atomic world. Moreover we will show how tomography can overcome the clouding effects of planar defects on structure identification by TEM.

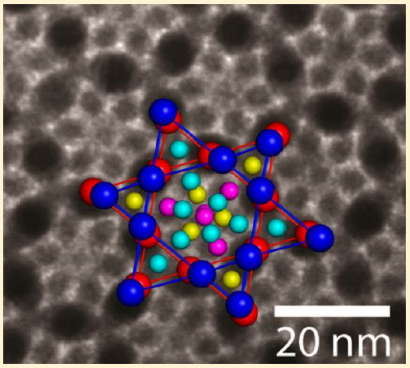

KEYWORDS: *Electron tomography, nanocrystals, self-assembly, superlattices*

As technology's demand for more sophisticated materials with versatile properties remains increasing, the interest for nanocrystal-based materials has grown rapidly over recent years. A cheap and versatile route for the preparation of these structures is the bottom-up approach based on self-assembly of colloidal nanocrystals. The versatility of this approach originates from two separated steps; first colloidal nanocrystals (NCs) of a metallic, semiconductor or magnetic compound are prepared from atomic precursors; second, any conceivable combination of these nanocrystals can be used to achieve binary nanocrystal superlattices (NCSL) by self-assembly.[1−3] In these systems, new properties can emerge from the quantum mechanical and dipolar interactions between the building blocks that are in close contact and ordered in three dimensions.[4−8] In order to understand the colloidal crystallization, and the electrical and optical properties of the resulting superlattices it is essential to characterize the superlattice structure in detail, including its deformations and crystal defects.

Previous studies have already shown that NCSL can be formed in a plethora of different crystal structures that are also known from the atomic world.[9] However, NCSL often show slight variations and distortions depending on the details of the self-assembly conditions.[8,10−12] This feature is very different from atomic lattices where even slight modulations referred to the ideal lattice structure are energetically forbidden due to the nature of the covalent and ionic bonding. The deformations and polymorphs present in self-assembled NCSL, though interesting from a purely scientific viewpoint, hamper the identification and classification of NCSL crystal structures. For instance, they result in blurring of both transmission images and of characteristic spots in scattering techniques.

Structural analysis based on transmission electron microscopy (TEM) has proven to be an important tool for progress in this field. For instance, by careful analysis of the superlattice structures formed by two types of semiconductor NC with different size and comparing these structures with the predictions of the hard-sphere model, it could be concluded that entropy can be an important driving force for the NC self-assembly.[13] Another example: the understanding of self-doping in a binary NCSL of PbTe and Ag_2Te NCs also required a detailed structural analysis.[14] Being a technique that provides direct and local information, TEM is the first choice for structural characterization of such systems. It has, however, the inherent drawback of being a projection method. This first of all means that (nearly) all information along the beam axis is lost, making it very difficult to study buried lattice defects and distortions. Furthermore, the TEM projections of self-assembled NCSL are, though astoundingly beautiful, often very complex and variable. As a consequence, the direct determination of the crystal structure by identification of different projection patterns has proven to be challenging.

Received: January 9, 2013
Revised: February 9, 2013
Published: February 12, 2013

   dx.doi.org/10.1021/nl400100c | *Nano Lett.* 2013, 13, 1312−1316

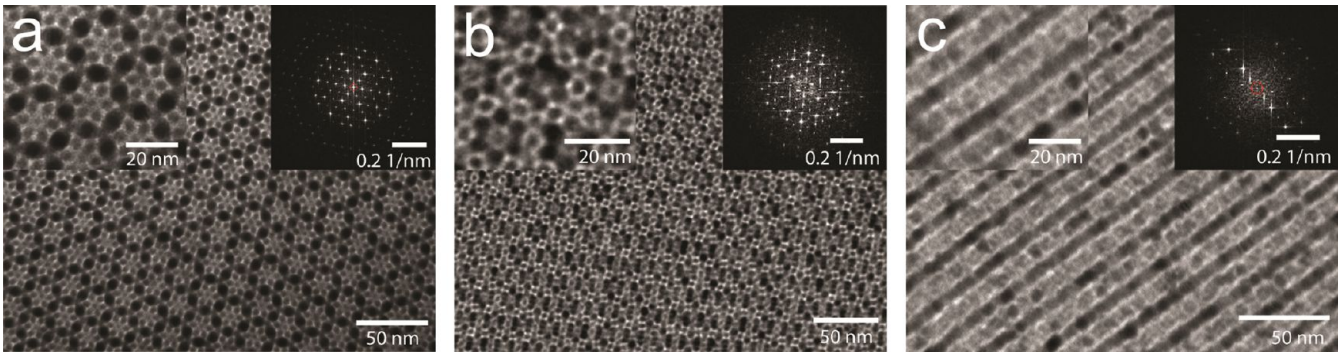

Figure 1. Various TEM pictures of nanocrystal superlattices optained in a particle size ratio range of 0.61−0.67. (a) Structure 1 showing clear hexagonal symmetry. (b) Structure 2 showing a more complex pattern but still hexagonal symmetry. (c) Structure 3 showing repetitions in 2 directions with no sign of hexagonal symmetry.

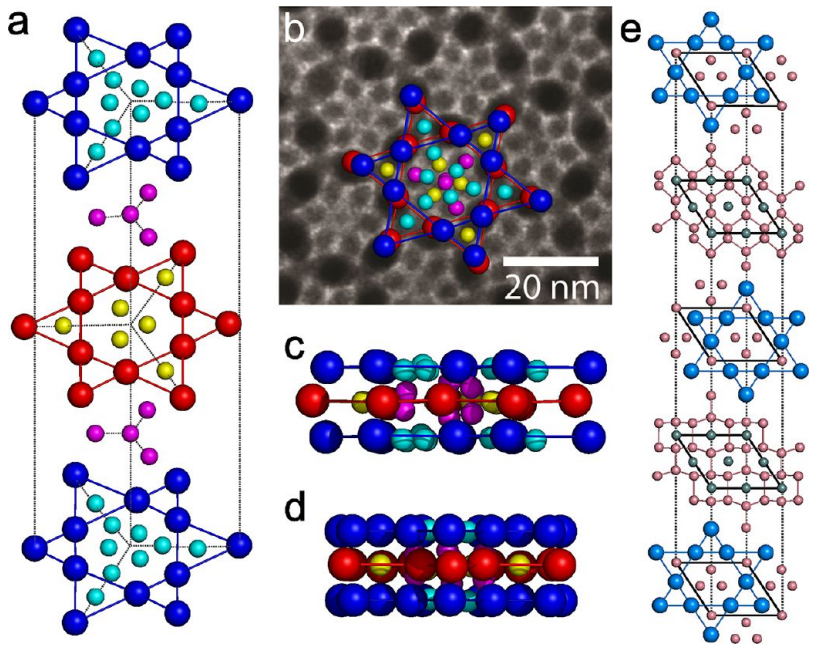

Figure 2. The A_6B_{19} structure. (a) The PbSe positions (large spheres) form an ABA stacking of a kagome-like structure with a 60° rotation between A (blue) and B (red). The CdSe positions (small spheres) form three different layers. The first layer (cyan) is in the same plane as the PbSe positions indicated in blue. The second layer (yellow) is in plane with the PbSe positions indicated in red. The third layer (purple) is located in between the PbSe layers, occupying one fcc position and three defect positions. Note that the spheres are not drawn to scale for better visibility. (b) Top view of the A_6B_{19} structure aligned with the TEM projection. (c,d) The respective side views of the structure. (e) Crystal structure of the $U_3Co_{12-x}Y_4$ (Y = Si, Ge) crystal, showing quite some resemblance to the A_6B_{19} structure described here. The primitive unit cell is indicated in black, U atoms in blue, Co atoms in pink, Si/Ge atoms in green.

In order to further our understanding of the formation and properties of self-assembled NCSL, a complete 3D structural characterization with a method that provides local information is highly desirable. In electron tomography, a three-dimensional reconstruction of a crystal structure is obtained from a series of 2D TEM projections acquired at different angles between the incoming electron beam and the lattice.[15,16] Hence, one can study the local three-dimensional structure of a lattice including the buried defects and boundaries. This has been demonstrated for binary as well as ternary NCSLs.[17−20]

Here, we show how electron tomography enabled us to resolve a complex crystal structure formed by self-assembly of PbSe and CdSe NCs. The structure has no analogue in the atomic world. Moreover, we show that the interpretation of TEM projections can be clouded by planar defects and misorientations in the superlattice but that this can be overcome by an analysis based on tomography. The observed superlattice structure resembles that of a jammed phase that can be simulated using mixtures of hard spheres with the same size ratio. However, modeling the structure with hard spheres results in a filling fraction considerably lower than that of a face-centered cubic (fcc) single component structure. This provides an indication that next to entropic, also enthalpic driving forces could play a role in the crystal structure formation (for a more elaborate discussion on this subject see the Supporting Information).[21−26]

Figure 1 shows different TEM projections taken from parts of self-assembled superlattices formed by the PbSe and CdSe NCs with a size-ratio range of 0.61−0.67. Figure 1a shows a clear hexagonally symmetric structure (structure 1), as is also confirmed by the clear pattern in the FFT (inset). Figure 1b (structure 2) shows features that are less sharp, resulting in a

dx.doi.org/10.1021/nl400100c | Nano Lett. 2013, 13, 1312−1316

much more diffuse FFT. However, still a hexagonal symmetry is observed. Figure 1c shows a superlattice (structure 3) that is under such an angle with the surface that almost no information about the structure can be extracted from the TEM image. These TEM images and other ones (see the Supporting Information) suggest that at this size-ratio PbSe and CdSe form several different superlattices, very different from our findings in other size-ratio regions where the same types of nanocrystals only lead to one or two binary crystal structures that were in agreement with predictions for hard-sphere mixtures.[13] Notice that these complex TEM images do not allow to identify the unit cell and crystal structure of these superlattices.

Using electron tomography and computer-aided particle detection, the average unit cell vectors for structure 1 can be estimated. The position of the larger PbSe NCs is relatively easy to find since the heavy Pb atoms lead to high image contrast. The large size of the PbSe NCs further facilitates the particle detection. Using the particle detection method as described in the Supporting Information, the positions of 466 individual PbSe NCs were determined. The unit vector distance between each of them was calculated and used to transpose all particles into one unit cell. This unit cell was then used to determine the relative positions of the smaller CdSe NCs. For the CdSe NCs, 1852 positions were determined. The relative distance to the unit cell's origin was used to transpose all determined positions into one unit cell. After this, their average position within the unit cell was calculated. The CdSe NCs are much harder to detect due to their smaller size and lower contrast in TEM − Cd is a much weaker electron scatterer than Pb. This results into a wider spread in the detected Cd positions. The final crystal structure is presented in Figure 2, and the coordinates of the primitive unit cell are presented in the Supporting Information. The structure has the remarkable stoichiometry of PbSe/CdSe 6:19. Looking at the structure in more detail, we can observe that the PbSe NCs form an ABA stacking of equivalent kagome-like lattices with three larger and three smaller triangles attached to a hexagon. Notice that the A (blue) and B (red) layers are rotated 60° with respect to each other, that is, the small triangles of layer A overlap with the large triangles of layer B. The CdSe NCs form an ABCBA stacking of three different hexagonally symmetric layers. Here A (cyan) and C (yellow) are in the same plane as the PbSe layers, and B (purple) occupies one fcc and three defect positions in between A and C. Using the above symmetry considerations and with the help of a dedicated software tool[27] we could assign the observed crystal structure to space group no. 187: $P\bar{6}m2$, for more details see the Supporting Information. The total volume of the unit cell is 5365 nm^3. Using the effective[28] radius of the NCs we find a packing fraction of 0.85. This dense stacking suggests that the crystal structure might be stable in the hard-sphere framework. However, it is to be noted that using the effective radius of the NCs is known to lead to an overestimation of the packing fraction due to the extra degree of freedom the NC ligands have in three dimensions with respect to two dimensions.[17]

We first used the particle coordinates as obtained from electron tomography and computer-aided particle detection in a Monte Carlo simulation of binary hard-sphere mixtures with a size ratio of 0.695. Upon compressing the system to high pressures, small particles moved out of position and the structure becomes disordered with a packing fraction of 0.641. Additionally, we performed Monte Carlo simulations with a variable box shape[29] to predict the crystal structure using the hard-sphere model. Statistical analysis of a large number of simulation cycles shows the predominant formation of a jammed phase with a packing fraction of 0.64. This jammed phase resembles the A_6B_{19} crystal structure with the position of the PbSe NCs mostly being preserved. However the positions of the CdSe NCs shift with respect to their position in the A_6B_{19} structure. For more information on the modeling see the Supporting Information. The outcome of the Monte Carlo simulations and the high packing fraction suggest that the observed crystal structure might be driven by both entropy and enthalpy, but further research is needed to clarify this point (also see the Supporting Information). We would like to remark that for the more complex structures with larger unit cells, like $NaZn_{13}$ and the Laves phases, the packing fraction of the structure alone is not an adequate measure anymore for the stability of the crystal. In fact, the Laves phases are with their packing fraction of 0.710 significantly below the 0.741 of the single component fcc structures. Nonetheless free energy calculations show that the Laves phases are stable in a size-ratio range of 0.76−0.84.[30] Furthermore it should be noted that, although no exact atomic equivalent was found, the crystal structure presented here shows resemblance to the $Gd_3Ru_4Al_{12}$ and the $U_3Co_{12-x}Y_4$ (Y = Si, Ge) structures, both of which are ternary variants of the $EuMg_{5.2}$ structure family (Figure 2e).[31−33]

Analyzing the electron tomogram of structure 2 (Figure 1b) directly shows the added value of electron tomography: a comparison of the reconstruction slices of the electron tomograms of structure 1 and 2 readily shows that they are actually the same structure in disguise. What makes the TEM images so different however (compare Figure 1a and 1b), is that a planar defect runs through the middle of structure 2 (Figure 3). This planar defect is in fact a stacking fault where the next kagome structure of PbSe NCs was not just rotated over 60°, but also translated by the small PbSe−PbSe distance over both the in-plane unit cell axes. Since the planar defect is located roughly in the middle of the crystal, both orientations contribute equally to the scattering of the electron beam. This results in a TEM picture showing a complicated pattern misleadingly pointing to two different crystal structures in Figure 1.

For structure 3 the particle positions were identified using the same procedure as for structure 1. The structure found was built up from the same kagome-like layers of PbSe with the difference that these layers are stacked under an angle of 43° with respect to the substrate (Figure 4). In earlier work by Smith et al.[34] and Friedrich et al.[17] drying forces resulting in strong compression in the direction of the surface normal were observed. In the present case however, the drying forces resulted in a lamellar offset of the different PbSe layers, thus distorting the crystal in the direction along the kagome layers rather than in the direction of the surface normal. The fact that the kagome layers are preserved hints toward stronger intralayer interactions than interlayer interactions, something that could also account for the stacking fault in structure 2. The lamellar distortion does not significantly influence the unit cell's volume, which is only 5.8% larger than the unit cell volume for structure 1. However, combined with the difference in orientation with respect to the electron beam it makes a trustful interpretation of the TEM image (Figure 1c) impossible.

dx.doi.org/10.1021/nl400100c | Nano Lett. 2013, 13, 1312−1316

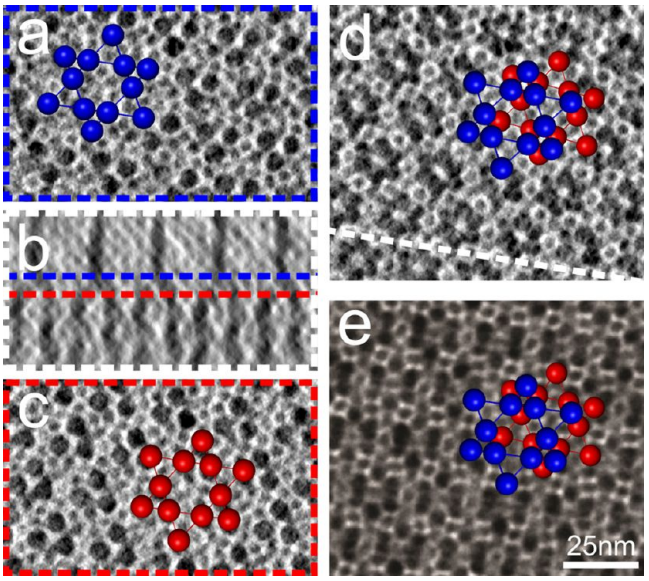

Figure 3. Tomographic reconstruction of structure 2. Horizontal reconstruction slices along the first PbSe layer above (a) and below (c) the planar defect. (b) A vertical reconstruction slice showing the planar defect and the position of the horizontal reconstruction slices. (d) Average of the two horizontal slices showing that the two PbSe kagome layers are not just rotated but also shifted with respect to each other. The white line indicates the position of the vertical slice (b). (e) the original TEM image of structure 2 showing the same pattern as (d).

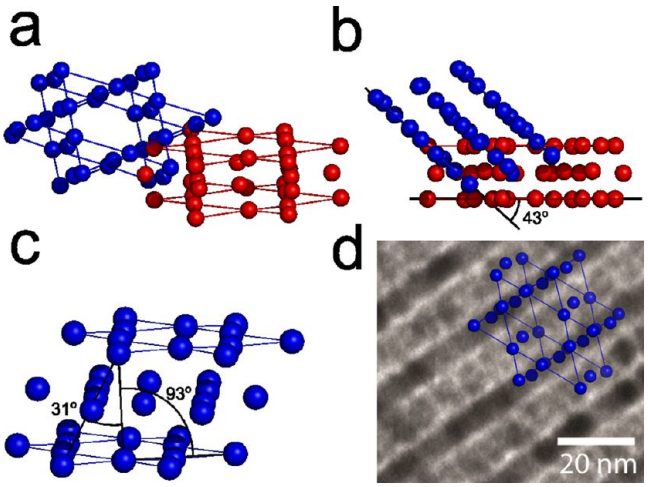

Figure 4. Analysis of structure 3. (a) Comparison of the distorted structure 3 (blue) with structure 1 (red). (b) The same layered kagome structure of the PbSe NCs is formed (blue), but the layer stacking direction is rotated 43° with respect to the stacking direction of structure 1 (red). (c) Drying forces acting on the crystal resulted in a lamellar displacement of the different PbSe layers. (d) Comparison of the detected unit cell to the TEM image.

PbSe and CdSe nanoparticles with a size ratio of 0.67 were found to assemble into a complicated binary nanoparticle superlattice, of which the structure could not be revealed by TEM. Electron tomography in combination with computer-aided particle tracking enabled us to determine the crystal lattice in three dimensions: the crystal with A_6B_{19} stoichiometry is formed by stacked layers of a kagome-like lattice of PbSe NCs with interstitial CdSe NCs. Furthermore, we find that three different and complex TEM images reflect the above structure. This work shows that electron tomography is an indispensable tool for the advanced study of nanocrystal solids, a very broad class of emerging nanostructured materials.

■ ASSOCIATED CONTENT

Ⓢ Supporting Information

Media files showing the raw tilt series (structure1_tilt.mpg (si_002), structure2_tilt.mpg (si_003), structure3_tilt.mpg (si_004)) and the corresponding 3D reconstructions (structure1_rec.mpg (si_005), structure2_rec.mpg (si_006), structure3_rec.mpg (si_007)) of the structures as labeled in Figure1, and a text file containing details on the NC synthesis and the computer aided particle detection, various TEM images of crystal structures observed at a size ratio range of 0.61−0.67, unit cell parameters of the A_6B_{19} crystal structure and details on the space group assignment and the Monte Carlo simulation. This material is available free of charge via the Internet at http://pubs.acs.org.

■ AUTHOR INFORMATION

Corresponding Author

*E-mail: d.vanmaekelbergh@uu.nl. Tel: (+31) 30-253-2218. Fax: (+31) 30-253-2403.

Present Address

[‖]W.H.E.: Kavli Institute of NanoScience, Delft University of Technology, Faculty of Applied Sciences, Loretzweg 1, 2628 CJ Delft, The Netherlands.

Author Contributions

[⊥]M.P.B. and W.H.E. contributed equally.

Notes

The authors declare no competing financial interests.

■ ACKNOWLEDGMENTS

This work was supported by FOM "Control over Functional Nanoparticle Solids (FNPS)". The manuscript was written through contributions of all authors. All authors have given approval to the final version of the manuscript.

■ REFERENCES

(1) Talapin, D. V.; Lee, J.-S.; Kovalenko, M. V.; Shevchenko, E. V. *Chem. Rev.* **2010**, *110*, 389−458.
(2) Rogach, A. L.; Talapin, D. V.; Shevchenko, E. V.; Kornowski, A.; Haase, M.; Weller, H. *Adv. Funct. Mater.* **2002**, *12*, 653−664.
(3) Vanmaekelbergh, D. *Nano Today* **2011**, *6*, 419−437.
(4) Overgaag, K.; Evers, W.; de Nijs, B.; Koole, R.; Meeldijk, J.; Vanmaekelbergh, D. *J. Am. Chem. Soc.* **2008**, *130*, 7833−7835.
(5) Redl, F. X.; Cho, K.-S.; Murray, C. B.; O'Brien, S. *Nature* **2003**, *423*, 968−971.
(6) Kiely, C. J.; Fink, J.; Brust, M.; Bethell, D.; Schiffrin, D. J. *Nature* **1998**, *396*, 444−446.
(7) Chen, Z.; Moore, J.; Radtke, G.; Sirringhaus, H.; O'Brien, S. *J. Am. Chem. Soc.* **2007**, *129*, 15702−15709.
(8) Shevchenko, E. V.; Talapin, D. V.; O'brien, S.; Murray, C. B. *J. Am. Chem. Soc.* **2005**, *127*, 8741−8747.
(9) Shevchenko, E. V.; Talapin, D. V.; Kotov, N. A.; O'Brien, S.; Murray, C. B. *Nature* **2006**, *439*, 55−59.
(10) Talapin, D. V.; Shevchenko, E. V.; Bodnarchuk, M. I.; Ye, X.; Chen, J.; Murray, C. B. *Nature* **2009**, *461*, 964−967.
(11) Ye, X.; Chen, J.; Murray, C. B. *J. Am. Chem. Soc.* **2011**, *133*, 2613−2620.
(12) Bodnarchuk, M. I.; Shevchenko, E. V.; Talapin, D. V. *J. Am. Chem. Soc.* **2011**, *133*, 20837−20849.
(13) Evers, W. H.; de Nijs, B.; Filion, L.; Castillo, S.; Dijkstra, M.; Vanmaekelbergh, D. *Nano Lett.* **2010**, *10*, 4235−4241.

(14) Urban, J. J.; Talapin, D. V.; Shevchenko, E. V.; Kagan, C. R.; Murray, C. B. *Nat. Mater.* **2007**, *6*, 115−121.
(15) Midgley, P. A.; Weyland, M. *Ultramicroscopy* **2003**, *96*, 413−431.
(16) Friedrich, H.; de Jongh, P. E.; Verkleij, A. J.; de Jong, K. P. *Chem. Rev.* **2009**, *109*, 1613−1629.
(17) Friedrich, H.; Gommes, C. J.; Overgaag, K.; Meeldijk, J. D.; Evers, W. H.; de Nijs, B.; Boneschanscher, M. P.; de Jongh, P. E.; Verkleij, A. J.; de Jong, K. P.; van Blaaderen, A.; Vanmaekelbergh, D. *Nano Lett.* **2009**, *9*, 2719−2724.
(18) Evers, W. H.; Friedrich, H.; Filion, L.; Dijkstra, M.; Vanmaekelbergh, D. *Angew. Chem., Int. Ed.* **2009**, *48*, 9655−9657.
(19) Florea, I.; Demortière, A.; Petit, C.; Bulou, H.; Hirlimann, C.; Ersen, O. *ACS Nano* **2012**, *6*, 2574−2581.
(20) Bals, S.; Casavola, M.; van Huis, M. A.; van Aert, S.; Batenburg, K. J.; van Tendeloo, G.; Vanmaekelbergh, D. *Nano Lett.* **2011**, *11*, 3420−3424.
(21) Hopkins, A.; Jiao, Y.; Stillinger, F.; Torquato, S. *Phys. Rev. Lett.* **2011**, *107*, 125501.
(22) Hopkins, A.; Stillinger, F.; Torquato, S. *Phys. Rev. E: Stat., Nonlinear, Soft Matter Phys.* **2012**, *85*, 021130.
(23) Filion, L.; Dijkstra, M. *Phys. Rev. E: Stat., Nonlinear, Soft Matter Phys.* **2009**, *79*, 046714.
(24) Hudson, T. S.; Harrowell, P. *J. Phys. Chem. B* **2008**, *112*, 8139−8143.
(25) Hudson, T. S.; Harrowell, P. *J. Phys.: Condens. Matter* **2011**, *23*, 194103.
(26) O'Toole, P. I.; Hudson, T. S. *J. Phys. Chem. C* **2011**, *115*, 19037−19040.
(27) Stokes, H. T.; Campbell, B. J.; Hatch, D. M. *FINDSYM*. stokes.byu.edu/iso/findsym.html 2013, (accessed Jan 30, 2013).
(28) The effective radius of the NCs is determined by measuring their centre to centre distance in hexagonally packed self-assembled monolayers using TEM. The effective radius therefore adds a reasonable estimation of the length of the organic ligand in self-assembled structures to the core radius of the inorganic NC.
(29) Filion, L.; Marechal, M.; Oorschot, B.; Pelt, D.; Smallenburg, F.; Dijkstra, M. *Phys. Rev. Lett.* **2009**, *103*, 188302.
(30) Hynninen, A.-P.; Filion, L.; Dijkstra, M. *J. Chem. Phys.* **2009**, *131*, 064902.
(31) Gladyshevskii, R. E.; Strusievicz, O. R.; Cenzual, K.; Parthé, E. *Acta Cryst. B* **1993**, *49*, 474−478.
(32) Soudé, A.; Tougait, O.; Pasturel, M.; Kaczorowski, D.; Noël, H. *J. Solid State Chem.* **2010**, *183*, 1180−1185.
(33) Erassme, J.; Lueken, H. *Acta Cryst. B* **1987**, *43*, 244−250.
(34) Smith, D. K.; Goodfellow, B.; Smilgies, D.-M.; Korgel, B. A. *J. Am. Chem. Soc.* **2009**, *131*, 3281−3290.

Supporting Information

Electron tomography resolves a complex and novel crystal structure in a nanocrystal assembly

*Mark P. Boneschanscher,[1,‡] Wiel H. Evers,[1,‡,†] Weikai Qi,[2] Johannes D. Meeldijk,[3] Marjolein Dijkstra,[2] and Daniel Vanmaekelbergh[1,]**

[1] Condensed Matter and Interfaces, Debye Institute for Nanomaterials Science, University Utrecht, Princetonplein 1, 3584 CC Utrecht, The Netherlands; [2] Soft Condensed Matter, Debye Institute for Nanomaterials Science, University Utrecht, Princetonplein 1, 3584 CC Utrecht, The Netherlands; [3] Electron Microscopy Group, Utrecht University, Padualaan 8, 3584 CH Utrecht, The Netherlands.

‡ These authors contributed equally.

† Present address: Kavli Institute of NanoScience, Delft University of Technology, Faculty of Applied Sciences, Loretzweg 1, 2628 CJ Delft, The Netherlands.

Table of content

I Details on the NC synthesis and the computer aided particle detection

Oleic acid capped PbSe and trioctylphosphine oxide/hexadecylamine capped CdSe NC were prepared according to literature.[1,2] The as prepared NCs had an inorganic core size of 6.5±0.4nm (PbSe) and 3.4±0.3nm (CdSe) and an effective size of 9.4±0.3nm (PbSe) and 5.8±0.3nm (CdSe). Effective sizes, giving an estimate for the contribution of the soft ligand shell, were determined by measuring the centre-to centre distance of the NCs in a hexagonally packed single-component monolayer.

The NCSL were prepared by solvent evaporation as reported previously.[3] In short, suspensions of the PbSe and CdSe NCs in tetrachloroethylene were mixed at concentration ratio of 1:4 PbSe:CdSe. Colloidal crystallization was achieved by evaporation of the solvent under reduced pressure (~10 mbar) and enhanced temperature (70 °C) while keeping the substrate (a Pioloform coated TEM-grid) under an angle of 30° to the horizon. All synthesis were performed in an nitrogen purged glovebox.

Electron tomography was performed in a similar way as described in depth in previous work.[4] Transmission images and tilt series were acquired in bright-field mode using a Tecnai 20 electron microscope with a LaB_6 electron source (FEI Company, Eindhoven). The tilt series were acquired over $\pm 65^{o}$ with a 1^{o} increment. The entire object was imaged in underfocus throughout the tilt series.

Particle detection was done using template matching in Matlab as described by Heiner et al.[4] Following on the particle detection a statistical analysis of the unit cell was performed. The unit vectors were determined by averaging over the nearest neighbor distances that were determined by a Voronoi analysis. Particle positions were then expressed as a distance from the origin of their respective unit cells. Averaging over these distances resulted in the final coordinates. Since the spread in the CdSe positions was very large we used an additional detection criterion. This was to only include positions that were separated over at least one CdSe diameter (inorganic core diameter) from other CdSe positions within the same unit cell.

II Various TEM images of crystal structures observed at a size ratio range of 0.61-0.67

For self-assembly of the NCs at a size ratio range of 0.61-0.67 various structures are observed that show long-range ordering (Figure S1). Although the grain size of the structures can go up to several micrometers, a lot of different structures are observed within 1 synthesis. An overview of some typical crystal structures/orientations observed on one TEM grid is shown in Figure S2.

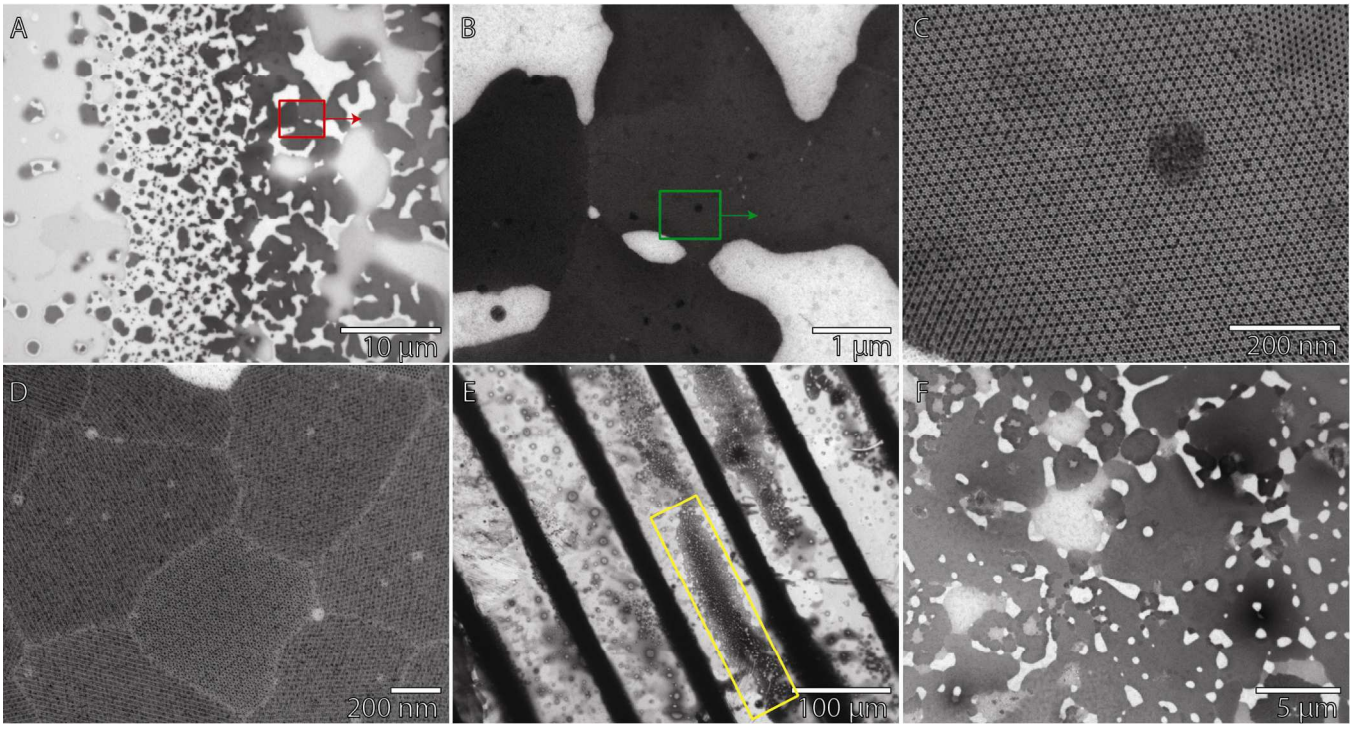

Figure S1. Typical overview TEM images of self-assembled NC superlattices in the size ratio of 0.61-0.67. (a-c) Various TEM images of the same region showing micrometer sized single domains of various crystal structures/orientations. (b) Zoom in on the red square in (a). (c) Zoom in on the green square of (b). (d) Various crystal domains with small grain sizes. (e) Large scale overview, where the region of the crystallites shown in (d) is indicated with the yellow box. (f) Zoomed in TEM image of (e) showing crystallites (dark patches) next to thin disordered regions (bright patches). Note that the average overall surface coverage of the various crystal structures in this size ratio is <1%

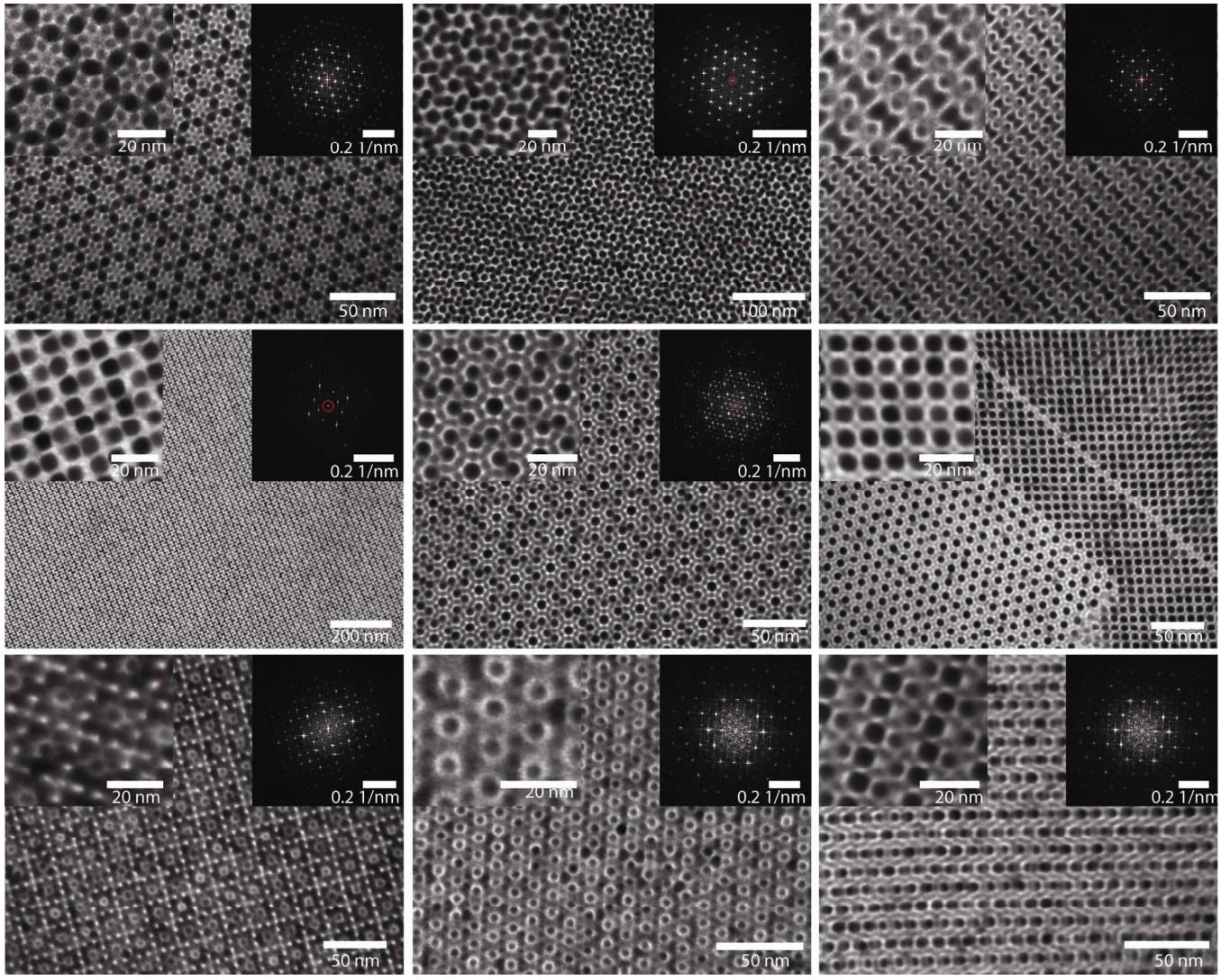

Figure S2. TEM images of (unknown) binary nanocrystal superlattices/orientations observed in the size ratio range 0.61-0.67. In the inset the FFT of the obtained superlattices is given. All structures are observed on one and the same TEM grid. The very first panel shows the TEM image of the structure discussed in the paper.

III Unit cell parameters of the A_6B_{19} crystal structure

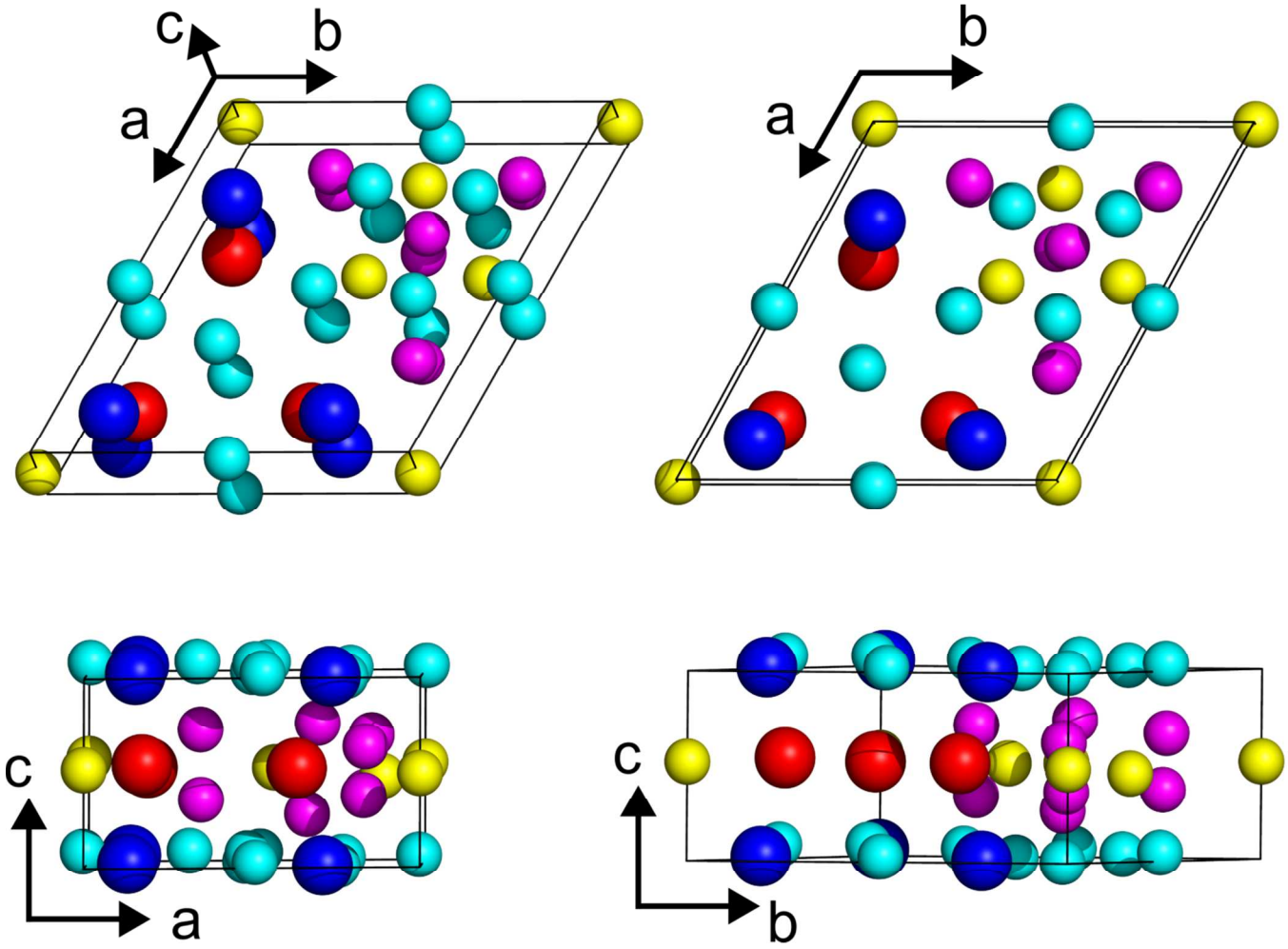

Figure S3. Three dimensional, top and different side views of the detected unit cell. Balls with the same color depict nanocrystals within the same layer. PbSe nanocrystals are displayed in blue and red, CdSe nanocrystals in cyan, magenta and yellow. The unit vectors are defined as **a** in the xy plane at an angle of -120^o with the x-axis, **b** along the x-axis and **c** along the z-axis.

Table S1. Lattice parameters given in Cartesian coordinates, lengths and angles.

Unit vector	x (nm)	y (nm)	z (nm)	Length (nm)	Angle (^{o})
a, α	-9.4 ± 0.7	-22.3 ± 0.6	-0.2 ± 0.8	24.2 ± 0.7	89.2 ± 2.8
b, β	22.4 ± 0.7	2.3 ± 0.8	-0.3 ± 0.7	22.5 ± 0.7	89.4 ± 1.8
c, γ	0.3 ± 0.9	-0.4 ± 0.9	11.2 ± 0.7	11.2 ± 0.8	118.7 ± 2.5

Table S2. The 25 unique nanocrystal positions within the unit cell given in both Cartesian coordinates and fractions of the unit vectors. Color coding refers to Figure S3.

Nanocrystal	x (nm)	y (nm)	z (nm)	a	b	c
PbSe (blue)	-5.1 ± 0.7	-19.3 ± 0.9	-0.2 ± 0.9	0.88 ± 0.03	0.14 ± 0.04	0.00 ± 0.08
PbSe (blue)	7.9 ± 0.7	-18.0 ± 0.9	-0.4 ± 0.6	0.88 ± 0.03	0.72 ± 0.04	0.00 ± 0.05
PbSe (blue)	0.6 ± 1.0	-5.7 ± 0.7	0.0 ± 0.6	0.27 ± 0.04	0.14 ± 0.03	0.01 ± 0.05
PbSe (red)	6.5 ± 1.0	-17.3 ± 0.9	5.4 ± 0.9	0.83 ± 0.04	0.63 ± 0.04	0.51 ± 0.08
PbSe (red)	0.6 ± 1.2	-8.3 ± 0.9	5.2 ± 0.9	0.38 ± 0.05	0.18 ± 0.04	0.48 ± 0.08
PbSe (red)	-3.8 ± 1.2	-18.3 ± 1.1	5.6 ± 1.0	0.83 ± 0.05	0.17 ± 0.05	0.52 ± 0.09
CdSe (cyan)	0.8 ± 1.0	-14.5 ± 0.7	0.4 ± 0.9	0.68 ± 0.04	0.32 ± 0.03	0.06 ± 0.08
CdSe (cyan)	6.1 ± 1.0	-10.5 ± 0.7	0.2 ± 0.9	0.52 ± 0.04	0.49 ± 0.03	0.04 ± 0.08
CdSe (cyan)	12.2 ± 1.0	-10.7 ± 0.7	10.6 ± 0.4	0.54 ± 0.04	0.76 ± 0.03	0.98 ± 0.04
CdSe (cyan)	-4.8 ± 1.0	-11.4 ± 0.7	0.3 ± 0.7	0.51 ± 0.04	0.00 ± 0.03	0.04 ± 0.06
CdSe (cyan)	8.9 ± 1.2	-4.4 ± 0.7	10.8 ± 0.7	0.23 ± 0.05	0.48 ± 0.03	0.98 ± 0.06
CdSe (cyan)	14.9 ± 1.0	-3.8 ± 0.9	-0.2 ± 0.7	0.25 ± 0.04	0.77 ± 0.04	0.01 ± 0.06
CdSe (cyan)	11.6 ± 1.2	1.0 ± 0.7	0.1 ± 1.0	0.01 ± 0.05	0.52 ± 0.03	0.02 ± 0.09
CdSe (magenta)	11.6 ± 0.7	-6.4 ± 0.7	2.4 ± 0.4	0.35 ± 0.03	0.66 ± 0.03	0.24 ± 0.04
CdSe (magenta)	6.1 ± 1.0	-3.1 ± 0.7	3.2 ± 0.8	0.17 ± 0.04	0.34 ± 0.03	0.30 ± 0.07
CdSe (magenta)	12.4 ± 1.0	-13.2 ± 0.7	3.6 ± 0.9	0.67 ± 0.04	0.83 ± 0.03	0.36 ± 0.08
CdSe (magenta)	17.1 ± 1.0	-2.0 ± 0.7	3.6 ± 0.9	0.17 ± 0.04	0.83 ± 0.03	0.35 ± 0.08
CdSe (yelow)	0.2 ± 1.0	-0.2 ± 1.1	5.6 ± 1.1	0.00 ± 0.04	0.00 ± 0.05	0.50 ± 0.10
CdSe (yelow)	8.6 ± 0.7	-8.7 ± 0.4	5.2 ± 0.4	0.44 ± 0.03	0.56 ± 0.02	0.49 ± 0.04
CdSe (yelow)	11.4 ± 1.0	-2.9 ± 0.7	5.2 ± 0.4	0.18 ± 0.04	0.58 ± 0.03	0.48 ± 0.04
CdSe (yelow)	15.7 ± 1.0	-8.0 ± 1.1	4.7 ± 0.7	0.44 ± 0.04	0.88 ± 0.05	0.45 ± 0.06
CdSe (magenta)	12.3 ± 1.0	-6.3 ± 0.9	7.8 ± 0.6	0.34 ± 0.04	0.68 ± 0.04	0.72 ± 0.05
CdSe (magenta)	6.1 ± 1.2	-3.1 ± 0.9	7.4 ± 0.8	0.16 ± 0.05	0.33 ± 0.04	0.67 ± 0.07
CdSe (magenta)	12.3 ± 1.0	-13.7 ± 0.7	6.6 ± 0.7	0.69 ± 0.04	0.83 ± 0.03	0.62 ± 0.06
CdSe (magenta)	17.3 ± 1.0	-2.3 ± 0.7	7.0 ± 0.6	0.18 ± 0.04	0.84 ± 0.03	0.65 ± 0.05

IV Space group assignment of the A_6B_{19} crystal structure

To assign the correct space group to the A_6B_{19} crystal structure the programme FINDSYM[5] was used. The unit vectors as given in Table S1 and the positions as given in Table S2 were used as input. As additional input parameters we used a tolerance of 1.7nm, a random centering and an hexagonal axes system. Using these tolerance settings, the symmetry operations possible showed that the A_6B_{19} structure can be classified in the $P\bar{6}m2$ space group (no. 187). Forcing this symmetry upon the structure, the occupation of the unit cell can be given in Wyckoff positions (Table S3).

Table S3. The nanocrystal positions within the unit cell when forcing $P\bar{6}m2$ symmetry. The unit cell vectors are **a** = **b** = 23.36nm, **c** = 11.21nm with $\alpha = \beta = 90^o$ and $\gamma = 120^o$. Color coding refers to Figure S3.

Nanocrystal	**a**	**b**	**c**
Wyckoff position j, x = -0.135			
PbSe (blue)	0.270	0.135	0.000
PbSe (blue)	0.865	0.135	0.000
PbSe (blue)	0.865	0.730	0.000
Wyckoff position k, x = -0.182			
PbSe (red)	0.363	0.182	0.500
PbSe (red)	0.818	0.182	0.500
PbSe (red)	0.818	0.637	0.500
Wyckoff position e			
CdSe (cyan)	0.667	0.333	0.000
Wyckoff position j, x = -0.497			
CdSe (cyan)	0.503	0.007	0.000
CdSe (cyan)	0.503	0.497	0.000
CdSe (cyan)	0.993	0.497	0.000

Wyckoff position j, x = 0.237			
CdSe (cyan)	0.237	0.473	0.000
CdSe (cyan)	0.237	0.763	0.000
CdSe (cyan)	0.572	0.763	0.000
Wyckoff position h, z = -0.260			
CdSe (magenta)	0.333	0.667	0.260
CdSe (magenta)	0.333	0.667	0.740
Wyckoff position n, x = 0.166, z = -0.345			
CdSe (magenta)	0.166	0.332	0.345
CdSe (magenta)	0.166	0.834	0.345
CdSe (magenta)	0.668	0.834	0.345
CdSe (magenta)	0.166	0.332	0.655
CdSe (magenta)	0.166	0.834	0.655
CdSe (magenta)	0.668	0.834	0.655
Wyckoff position b			
CdSe (yellow)	0.000	0.000	0.500
Wyckoff position k, x = 0.430			
CdSe (yellow)	0.140	0.570	0.500
CdSe (yellow)	0.430	0.570	0.500
CdSe (yellow)	0.430	0.860	0.500

Comparing the measured crystal structure with the structure after forcing $P\bar{6}m2$ symmetry we note that, in order to force the $P\bar{6}m2$ symmetry we had to move the particles over distances that fall well below the standard deviation in our measurement as presented in Table S2 (see also Figure S4). We therefore conclude that the deviation of the measured crystal structure from $P\bar{6}$ $m2$ symmetry is more likely to be a measurement error than a physical phenomenon.

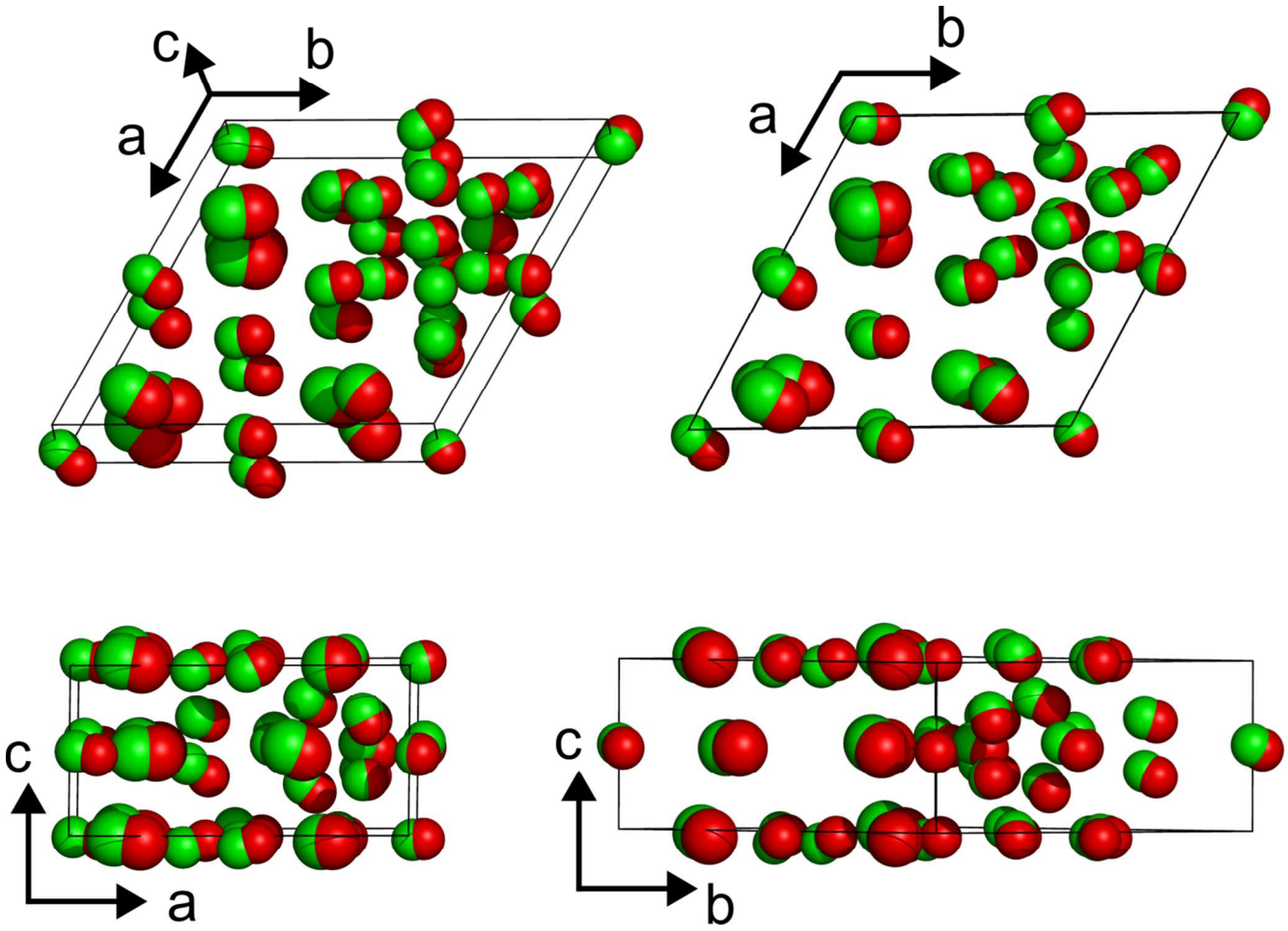

Figure S4. Comparison of the detected unit cell before (green) and after (red) forcing $P\bar{6}m2$ symmetry. Note that the balls are not drawn to scale. The shift in position in order to force $P\bar{6}m2$ symmetry is well below the standard deviation of the measured positions.

V Monte Carlo simulation of the A_6B_{19} structure

To evaluate whether the experimentally observed A_6B_{19} structure is stable for a binary mixture of hard spheres, Monte Carlo (MC) simulations were performed (Figure S5a). The configuration of the experimental results and a size ratio of 0.695 were used as initial parameters for the simulations. Subsequently the system was compressed to a higher pressure of PV/kT= 1000000.0 using 300000 MC steps. The densest packing fraction obtained in our simulation is 0.641. Although this is higher than the experimental values for the inorganic cores only, it is still much below the 0.85 we find with the effective sizes. Figure S5b shows the densest structure obtained in our simulations. Compared to the experimental configuration, some of the small particles moved out of position and the structure becomes more disordered. If the particles are only allowed to move in the xy direction, the A_6B_{19} structure seems to be stable. The maximum packing fraction obtained in this case is 0.575.

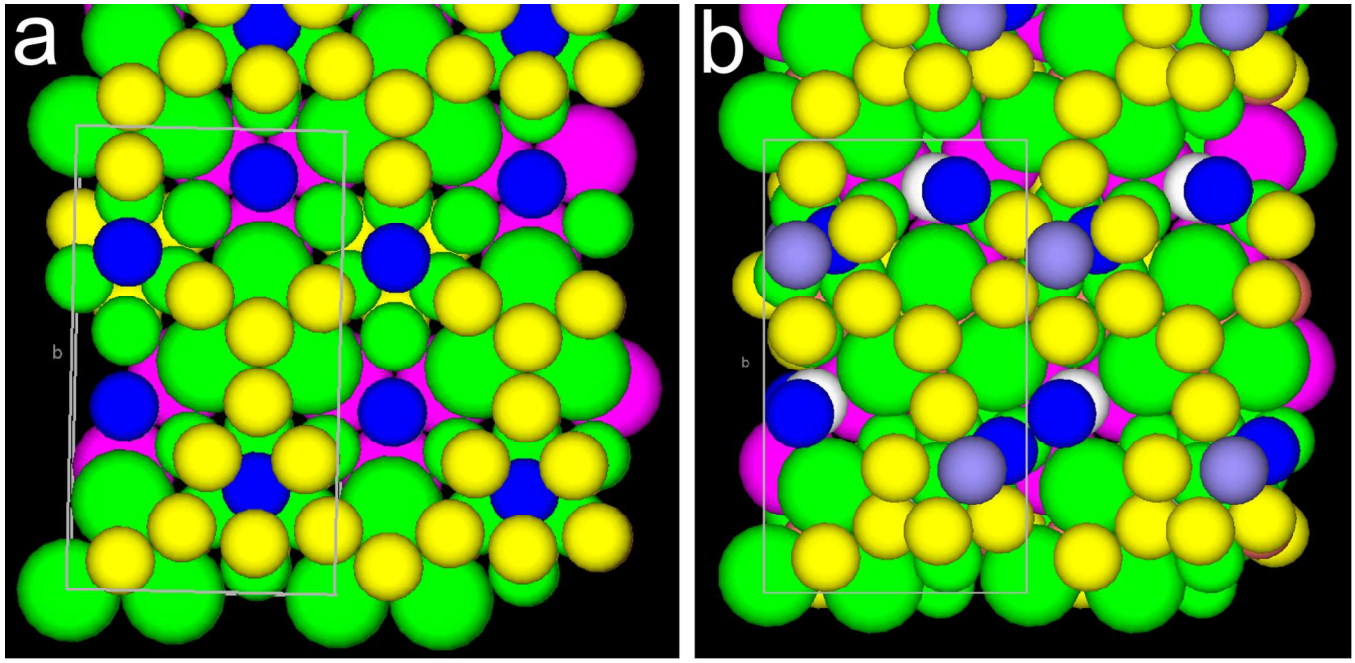

Figure S5. (a) Top view of the A_6B_{19} initial configuration obtained from experiment. The color coding of the particles corresponds to the particular height of their center of mass. (b) Densest packing structure obtained by MC simulations.

To assess the crystal structures and densest packing fraction at various size ratios in a range of 0.61-0.72, floppy box simulations were performed on 25 particles (6 large and 19 small particles) in a unit cell.[6] In floppy box simulations, the shape of the unit cell is allowed to vary in order to fit the possible crystal structures. After 100 independent simulations we observed a variation of the densest packing fraction in the range of 0.668-0.686 as a function of size ratio (Figure S6). However, due to the amount of particles in the unit cell (25), the particles packed into a disordered jammed structure as for example given in Figure S7.

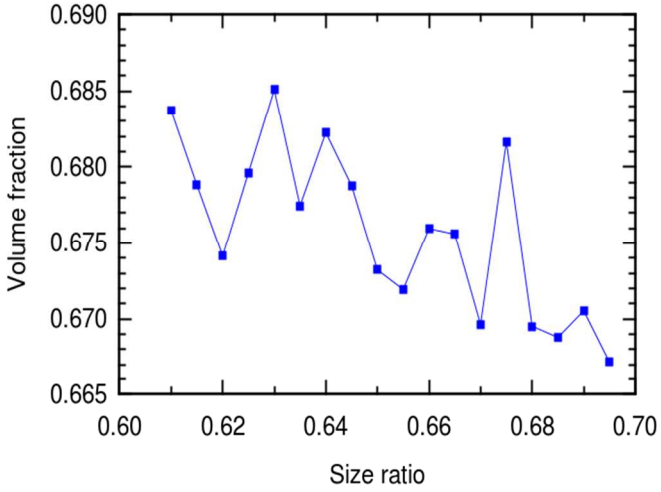

Figure S6. Densest obtained volume fraction as a function of particle size ratio.

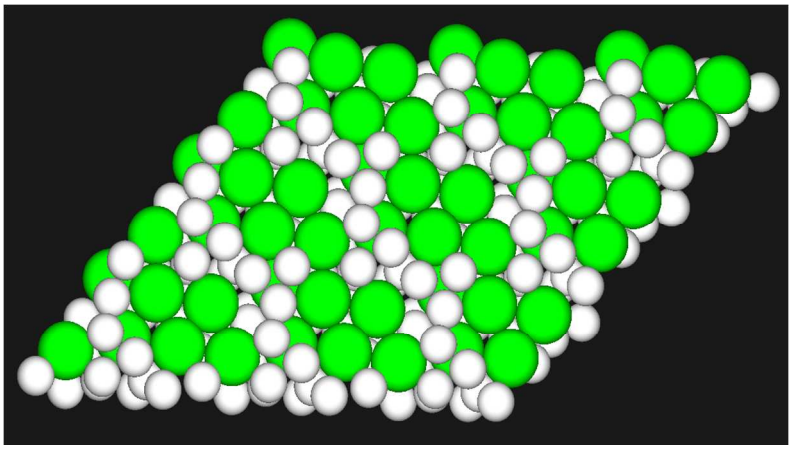

Figure S7. Disordered packed structures obtained by floppy box simulations. The PbSe positions are indicated in green and the CdSe positions in white.

Our finding that MC simulations with hard spheres are unable to reproduce the experimentally found structure can be attributed to complications in the modelling due to the large system size. On the other hand, this finding may point out that the system actually cannot be modelled with hard spheres anymore. This would imply that the formation of the observed crystal structure cannot be explained by entropy alone. If this is true, than it would be counterintuitive with our earlier work[3] where we describe how, for exactly the same nanocrystals and the same chemical environment, we mainly do find superlattice structures of which the formation can be explained with entropy only. We would like to point out however, that in the size ratio regime of 0.61-0.67 used in this study, no stable structures of hard spheres have been predicted. As such, the formation of the crystal structure described in this work does not need to compete with entropy driven crystallization. Therefore we do not think that the enthalpic interaction between the nanocrystals necessarily needs to be large to explain the observed superlattice crystal structure. Rather, we think that enthalpy plays a bigger role in this superlattice crystal formation, simply due to the lower entropic contribution.

In order to find out if enthalpic interactions would stabilize the observed crystal structure, further research is necessary. A MC study of the system using slightly attractive and repulsive potentials between the particles would be recommendable, but falls beyond the scope of the present work. More detailed modelling of the system will however be complicated since the overall interaction potential between the NCs will be influenced by, among others, steric hindrance of the capping ligands, (screened) Van der Waals interaction between the NCs and residual charges on the NC surface or in solution.

VI References

(1) Houtepen, A. J.; Koole, R.; Vanmaekelbergh, D.; Meeldijk, J.; Hickey, S. G. *J. Am. Chem. Soc.* **2006**, *128*, 6792-6793.

(2) de Mello Donegá, C; Hickey, S. G.; Wuister, S. F.; Vanmaekelbergh, D.; Meijerink, A. *J. Phys. Chem. B* **2003**, *107*, 489-496.

(3) Evers, W. H.; de Nijs, B.; Filion, L.; Castillo, S.; Dijkstra, M.; Vanmaekelbergh, D. *Nano Lett.* **2010**, *10*, 4235–4241.

(4) Friedrich, H.; Gommes, C. J.; Overgaag, K.; Meeldijk, J. D.; Evers, W. H.; de Nijs, B.; Boneschanscher, M. P.; de Jongh, P. E.; Verkleij, A. J.; de Jong, K. P.; van Blaaderen, A.; Vanmaekelbergh, D. *Nano Lett.* **2009**, *9*, 2719–2724.

(5) Stokes, H. T.; Campbell, B. J.; Hatch, D. M.; *FINDSYM*, stokes.byu.edu/iso/findsym.html **2013**.

(6) Filion, L.; Marechal, M.; Oorschot, B.; Pelt, D.; Smallenburg, F.; Dijkstra, M.; *Phys. Rev. Lett.* **2009**, *103*, 188302.